

Synthesis and characteristics of screen printed ZnO thick films nanostructures grown using different methods

Osama Abdul Azeez¹ · Raad S. Sabry¹ · Marwa Abdul Muhsien Hassan¹ · Safaa Farhood Madlul¹

Received: 24 October 2014 / Accepted: 12 March 2015 / Published online: 1 April 2015
© The Author(s) 2015. This article is published with open access at Springerlink.com

Abstract Zinc oxide nanostructures prepared using two different methods: first method (simple evaporation) with different flow rates of (100, 200 and 300) (sccm) using a mixture of (Ar + O₂) with a ratio of (10:1). The second method (hydrothermal) zinc nitrate aqua solution and Teflon lined stainless steel autoclave was used as a reactor. The ZnO powders were deposited on different substrate using screen print technique also the conducting electrodes deposited by the same technique which is simple low cost and eligible for mass production. Field emission scanning electron microscope, Atomic force microscope was used to study surface morphology of the films and X-Ray diffraction to study the structural properties of the films. Also the electrical properties of the n-ZnO/p-Si devices were investigated.

1 Introduction

Metal-oxide semiconductors (MOS) had a great amount of attention for their applications in several areas such as medical diagnosis, toxin gases sensors and opto-electronic industries [1, 2]. Recently the Nano-structured materials appeared to show higher sensitivity due to their single crystalline Nanostructure, the gain in the ratio of the surface to volume and other physical properties [3, 4]. ZnO is one of the (MOS) materials that played a good role in different applications in electronic sensors and opto-electronic devices due to many advantages such as low cost,

having a good electronic mobility, and showing a good thermal and chemical stability [5, 6]. ZnO is one of the II–VI semi-conductors, it has a direct wide band gap -3.37 eV and excitation energy (60 meV) [7, 8], has great attention for researchers because of its optical properties which make it important material in many applications such as optical waveguides, transparent conducting coatings and optical detector devices [9]. Since the control of the size and shape of nanostructure materials plays main role and great effect on the physical properties of the materials, several methods and techniques are used to synthesize different materials including ZnO Nanostructures, such as Pulse laser deposition (PLD), Chemical vapor deposition (CVD), Chemical bath deposition (CBD), Hydrothermal and chemical reactions. Among these methods, the simple evaporation method is preferred due to its low cost and high quality products [10].

1.1 Method section

1.1.1 Simple evaporation method

First of all, silicon wafer with (100) orientation was cleaned carefully by standard procedures, first the silicon is cut in (1 cm × 3 cm) pieces wafer was dipped in a solution of 10 ml of byroxid and 10 ml NH₃OH and 50 ml of distilled water and heated for 10 min to 70 °C. The second step is dipping the Si wafer in 50 ml of distilled water with 10 ml of HCl and hated to 70 °C, finally the Si wafer dipped for 1 min in a mixture of Hf and distilled water with ratio 1:10 Then the silicon wafer is washed and dried. The silicon wafer calceniede in a box furnace to 1000 °C for 4 h. A layer of SiO₂ was obtained on the Si substrate. The preparation of ZnO nanostructure is carried out in a single stage controllable horizontal tube furnace (40 cm) with a

✉ Marwa Abdul Muhsien Hassan
osama_bd@yahoo.com

¹ Physics Department, College of Sciences, Al-Mustansiriya University, Baghdad 00964, Iraq

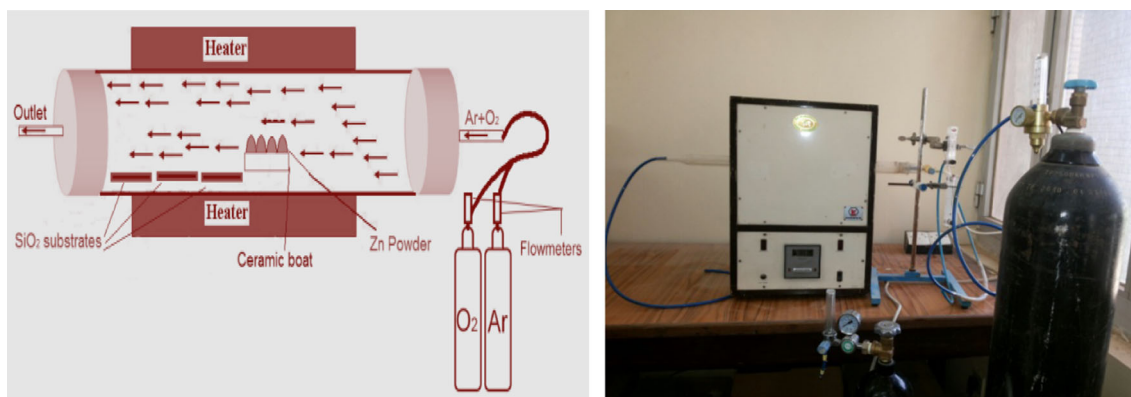


Fig. 1 schematic of simple evaporation system

quartz tube (50 cm) long and (3 cm) in diameter. A pure metallic Zinc powder (merck) Germany (99.9 %) is used as a raw material. (1 gm) of Zinc powder is placed in ceramic boat (1 × 1 × 10 cm). The boat was placed at the center of the tube furnace and the Si/SiO₂ substrates are positioned down the stream of the gas flow. Figure 1 shows a diagram of the system used to prepare the Zinc oxide. Before increasing temperature the quartz tube is purified from residual gases using pure Argon for 3 min, then we increase the temperature inside the furnace to 700 °C with gas mixture (Ar + O₂) flowing at a rate of (100, 200 and 300) (sccm) with a ratio of (10:1). The flow of gases was controlled by two flow meters. White cotton like powder is deposited on the substrates and the wall of the quartz tube. The whole process takes about 1 h. Then the furnace is left to cool down naturally to collect the product.

1.1.2 Hydrothermal method

All raw materials were analytical grade (>99 % shaula Spain) ZnO nanorods were synthesized using a simple hydrothermal method without catalysts or buffer layer. 2.231gm (0.5 M) of hexahedral zinc nitrates Zn(NO₃)₂·6H₂O were dissolved in 15 ml of deionized water, an equal volume of NaOH (3 M) was added to the aqua solution and stirred for 10 min, a white suspension appeared then 0.3gm of DE fructose was added to the mixture under stirrer for 1 h without heat, then the suspension was transferred into a Teflon lined stainless steel autoclave with a volume of 50 ml, the autoclave was sealed and kept at 160 °C for 12 h on hot plate stirrer with slow stirring. After that the autoclave cooled down to room temperature. The obtained powder washed several times in ethanol and distilled water. A proper amount of PVA was mixed with the prepared powder to make a paste, the paste screen printed in a pattern of 1 cm square thick films, the screen printed thick films dried at 120 °C for 30 min then heated at 500 °C for 1 h to remove residual organic materials. The prepared

thick films were examined by X-Ray diffraction (miniflex II Rigaku, Japan) (Cu, $\kappa\alpha$), Atomic force microscope (AFM) to study the morphology of the film surface and Field emission scanning electron microscope (Hitachi S-4160) (FESEM) to study the structural properties of the films. Also the optical behavior of the film was studied with UV-Visible light studied using shimadzu UV-Visible spectrophotometer.

2 Thick film preparation

The product is collected carefully. A proper amount of PVA (or any organic binder) is used to make the ZnO-PVA paste. The paste is screen printed in (1 cm) square pattern on different pre-cleaned substrates (glass, Si, SiO₂), the screen print is a simple technique to prepare the thick films with exact pattern and then the thick films are dried in air then, heated in a box furnace to 500 °C with a rate of 8 °C/min for 1 h to remove the organic material. Then the films were examined by different devices to study its structural properties. Ohmic contacts were fabricated on P type Si (1–10 Ω .cm) by evaporating 99.999 purity aluminum wires for backcontact for (I–V) measurements using Edwards coating system. A boat of tungsten was used to include the evaporated source, while finger integrated electrodes were screen printed on the thick film using silver paste. Figure 2 illustrates 11-finger interdigitated electrode IDE metal masks which were utilized in this work.

3 Results and discussion

In order to understand the structural properties of ZnO film samples prepared at different method, the X-ray diffraction study was carried out. X-ray diffraction analysis of ZnO film samples were carried out in the 20–80° range using Cu $\kappa\alpha$ radiation. Figures 3 and 4 shows an XRD pattern of

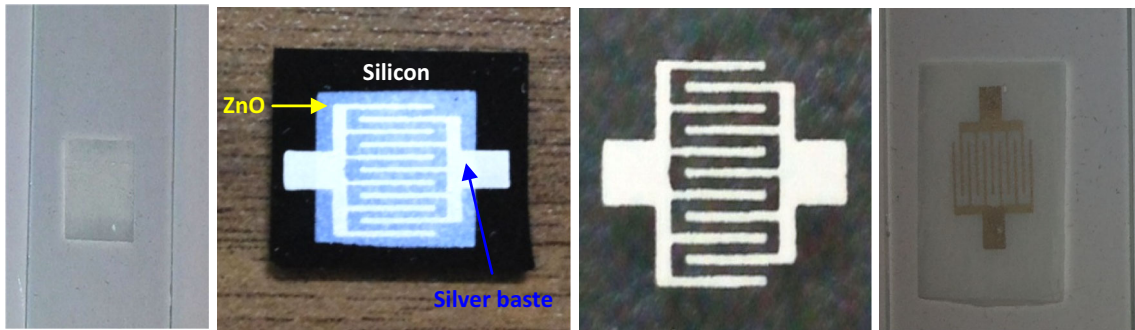


Fig. 2 schematic diagram of the IDE masks utilized in this work

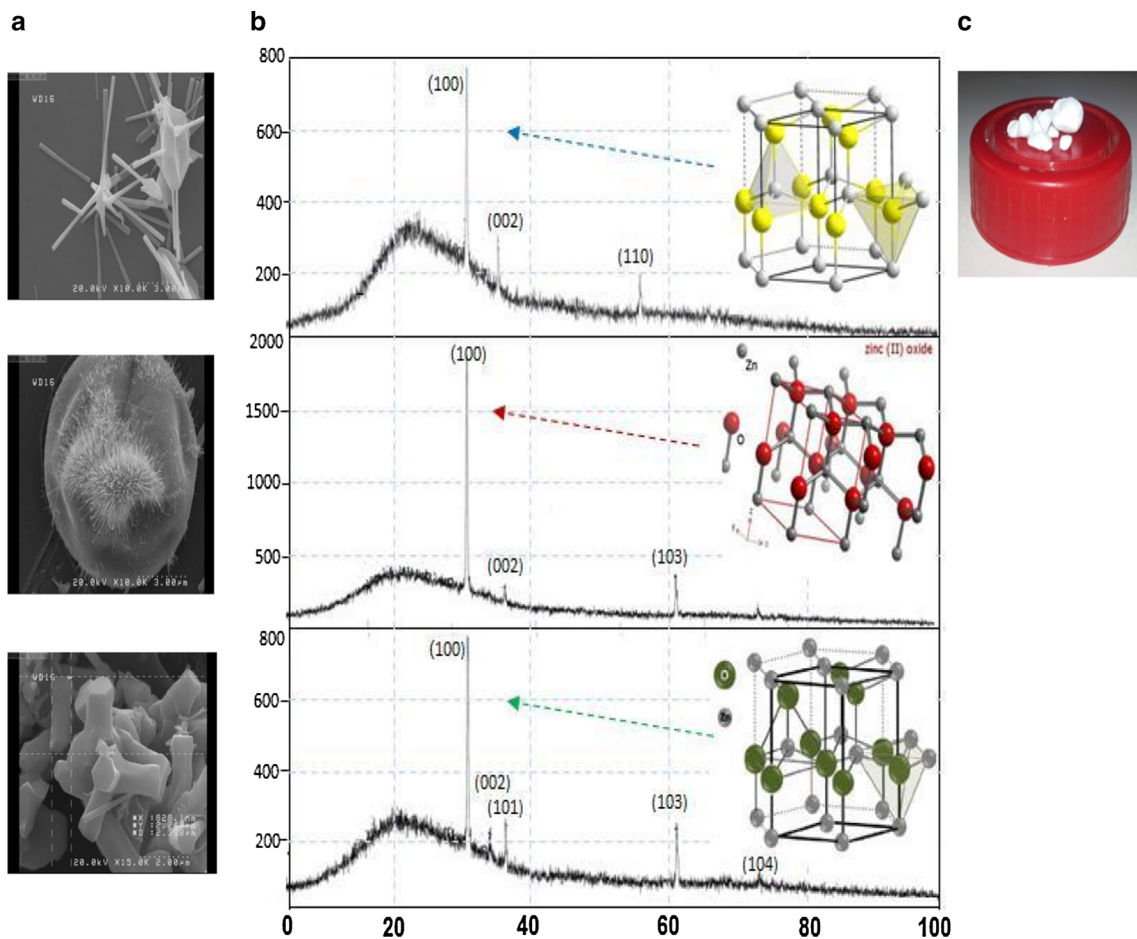
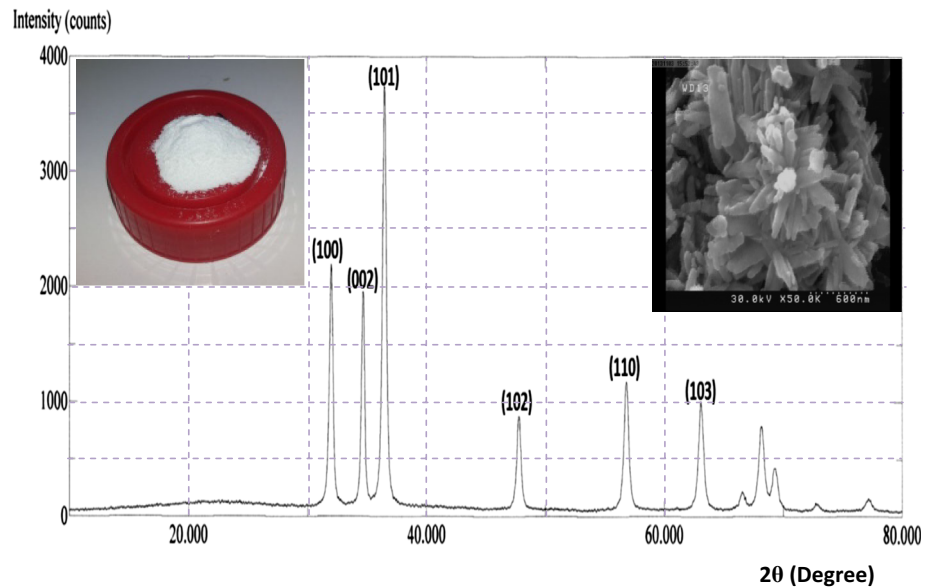


Fig. 3 XRD pattern of ZnO screen printed thick films prepared using simple evaporation system at **a** 100 sccm, **b** 200 sccm and, **c** 300 sccm flow rate mixture gas ($O_2 + Argon$)

ZnO film samples plotted in the range $20\text{--}80^\circ$ (2θ) versus intensity having several peaks of zinc oxide indicating random orientation for the polycrystalline nature and measured interplanar distances agreed with the values reported for ZnO in the literature. The observed peaks match well with the reported ASTM data of Zinc oxide, confirming the polycrystalline nature. The higher peak

intensities of an XRD pattern is due to the better crystallinity and bigger grain size can be attributed to the agglomeration of particles. The average crystallite size was calculated using Scherer equation and was estimated to be about 20–30 nm. The crystallinity of as prepared sample was characterized using XRD as shown in Figs. 3 and 4. The sharp diffraction pattern indicates that the sample

Fig. 4 XRD pattern of ZnO screen printed thick film prepared using hydrothermal method



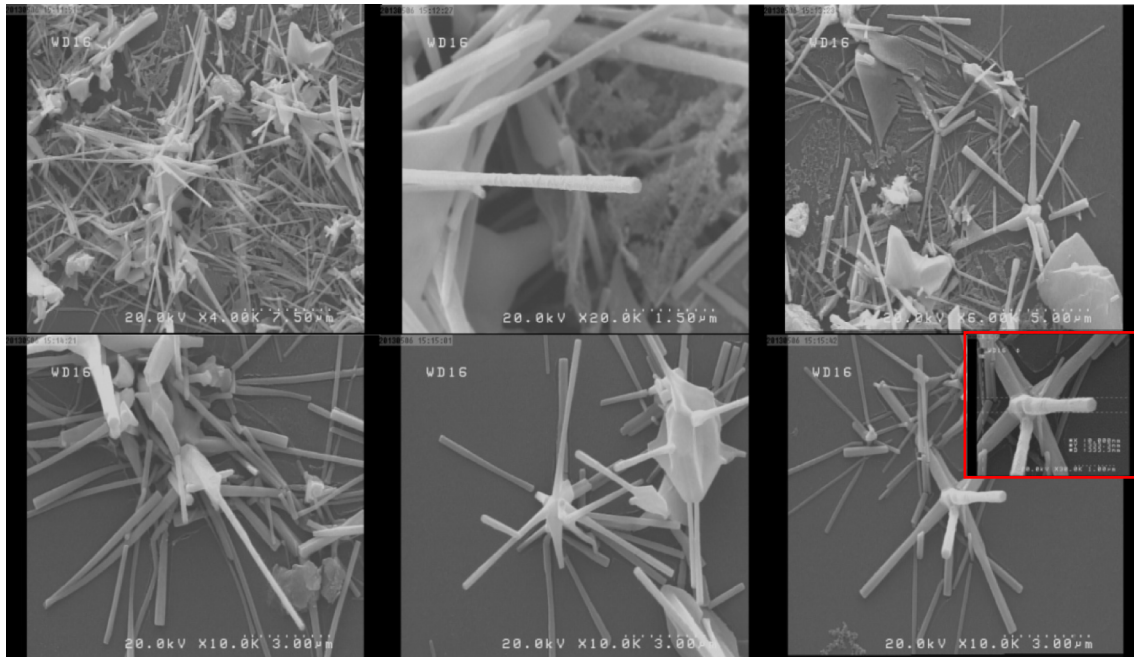
exhibits hexagonal ZnO crystalline structure with lattice constant of $a = 3.256 \text{ \AA}$ and $c = 5.31 \text{ \AA}$ which is reported in JCPDS (36–1451) for bulk ZnO. The diffraction pattern shows strong peak at (100) and (101) plane which confirms that great amount of nanostructure has aligned on the substrate and grown with orientation along the c axis. However no diffraction peak from elemental Zn was found in the samples. The diffraction patterns reveal good crystalline quality without any appreciable changes from pure ZnO films and are genuinely polycrystalline with a hexagonal wurtzite structure. All the peaks are in good agreement with the Joint committee on powder diffraction standard (JCPDS) data belonging to hexagonal ZnO structure. The corresponding reflecting planes are (100), (002), (101), (102), (110) and (103) respectively. The XRD patterns of all the samples indicated enhanced intensities for the peaks corresponding to (002) and (101) planes, indicating preferred orientation along the c -axis.

The simple evaporation is a direct method is to heat up Zn powder under oxygen flow. This method facilitates relative low growth temperature ($500\text{--}700 \text{ }^\circ\text{C}$), but the ratio between the Zn vapor pressure and oxygen pressure needs to be carefully controlled in order to obtain desired ZnO nanostructures. It has been observed that the change of this ratio contributes to a large variation on the morphology of nanostructures. According to the difference on nanostructure formation mechanisms, the extensively used vapor transport process can be categorized into the catalyst free vapor–solid (VS) process and catalyst assisted vapor–liquid–solid (VLS) process. Synthesis utilizing VS process is usually capable of producing a rich variety of nanostructures, including nanowires, nanorods, nanobelts and other complex structures. In a typical VS process, complex

ZnO nanostructures such as nanohelices and nanobelts were synthesized. In this process, in the VS process, the nanostructures are produced by condensing directly from vapor phase. Although multiple nanostructures can be obtained, this method obviously provides less control on the geometry, alignment and precise location of ZnO nanostructures. Many parameters affect the structure obtained by this method such as flow rate, evaporation temperature and the inert gas as the vapor carrier. In this work the temperature were fixed and the inert gas was Argon, the flow rate of the mixture ($\text{Ar} + \text{O}_2$) were change (100, 200, and 300) sccm per minute. For flow rate 100 sccm as shown in Fig. 5a the dominate structure obtained was tetra pod with different diameters and lengths also high porosity can be observed. While for flow rate 200 sccm Fig. 5b the dominate structure obtained was Urchin like and nano rods, a flower like minor structure was appeared. For flow rate 300 sccm Fig. 5c a hexagonal rods were the dominate structure obtained and a plain like minor structure was appeared, which grow only under a certain oxygen gas flow for a designated growth temperature and this oxygen flow rate increases with increasing the ratio of Ar-O_2 flow rate and also depends on the diameter of the quartz tube. The variation in oxygen gas flow is crucial since it can directly affect the process of oxidation of the Zn vapor and therefore, the growth characteristics. It is understood that, with increase in, the amount of evaporated Zn flux should increase thus an increased amount of oxygen source is required to maintain a particular Zn/O ratio which favors ZnO nanonail growth at $700 \text{ }^\circ\text{C}$ [11, 12].

Figure 6 shows the ZnO surface morphology of as synthesized sample prepared using hydrothermal method on a glass substrate. The morphology of these structures

A: 100 sccm



B: 200 sccm

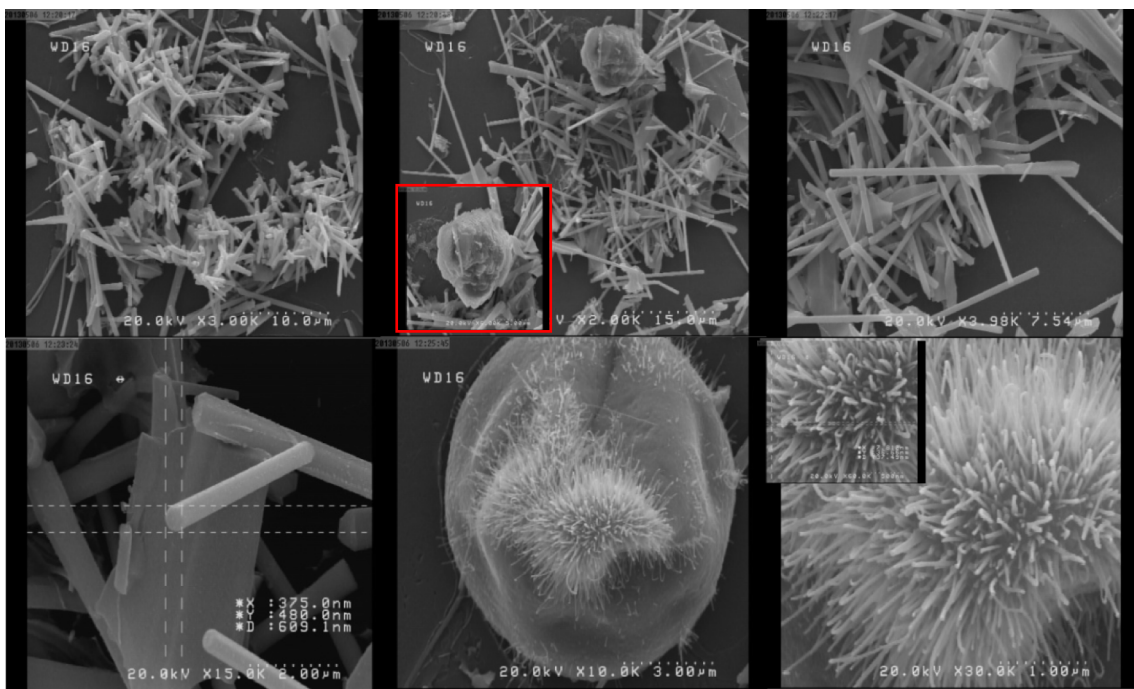


Fig. 5 FESEM of ZnO screen printed thick film prepared using simple evaporation system at **a** 100 sccm, **b** 200 sccm and, **c** 300 sccm flow rate

resembles that of nanorods. The length of these nanorods lies in the range of 100 nm with an average tip diameter of 60 nm and a base diameter of ≈ 50 nm as shown in these figure. All SEM images with different magnifications, some selected images will be presented and discussed to

show the effect of different condition on the sample parameters mentioned above (Table 1).

It is known that the surface properties of the transparent conducting oxide films influence their optical and electrical properties which are important factors for applications in

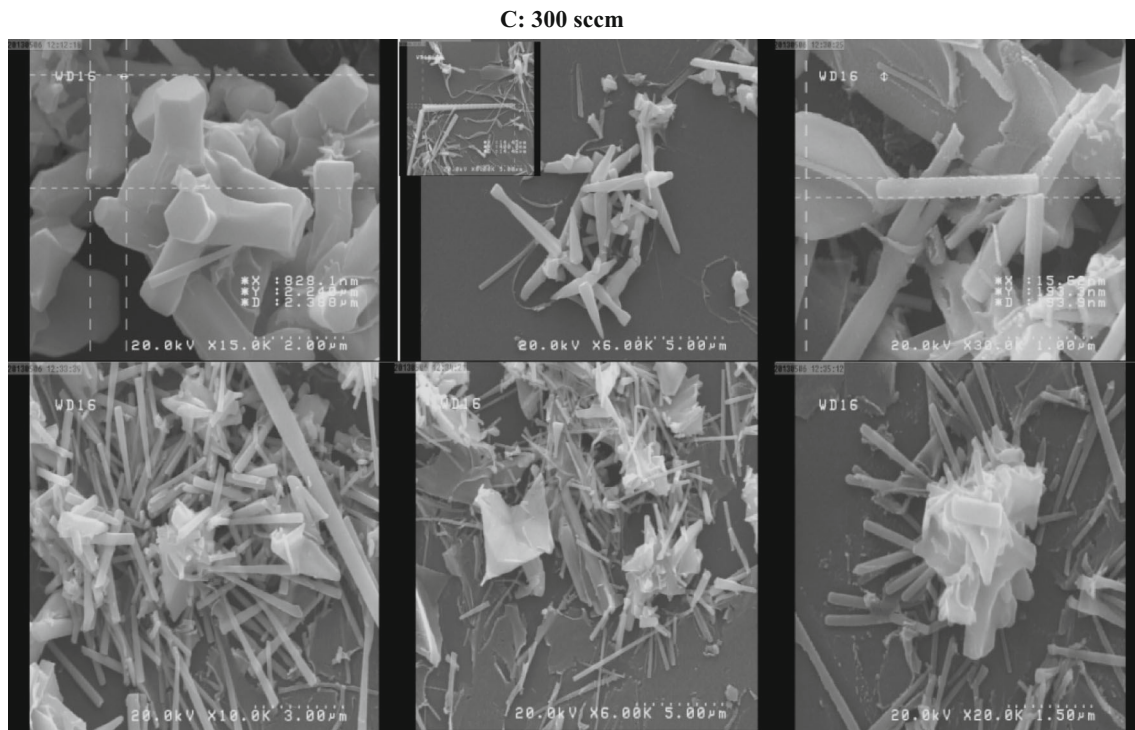


Fig. 5 continued

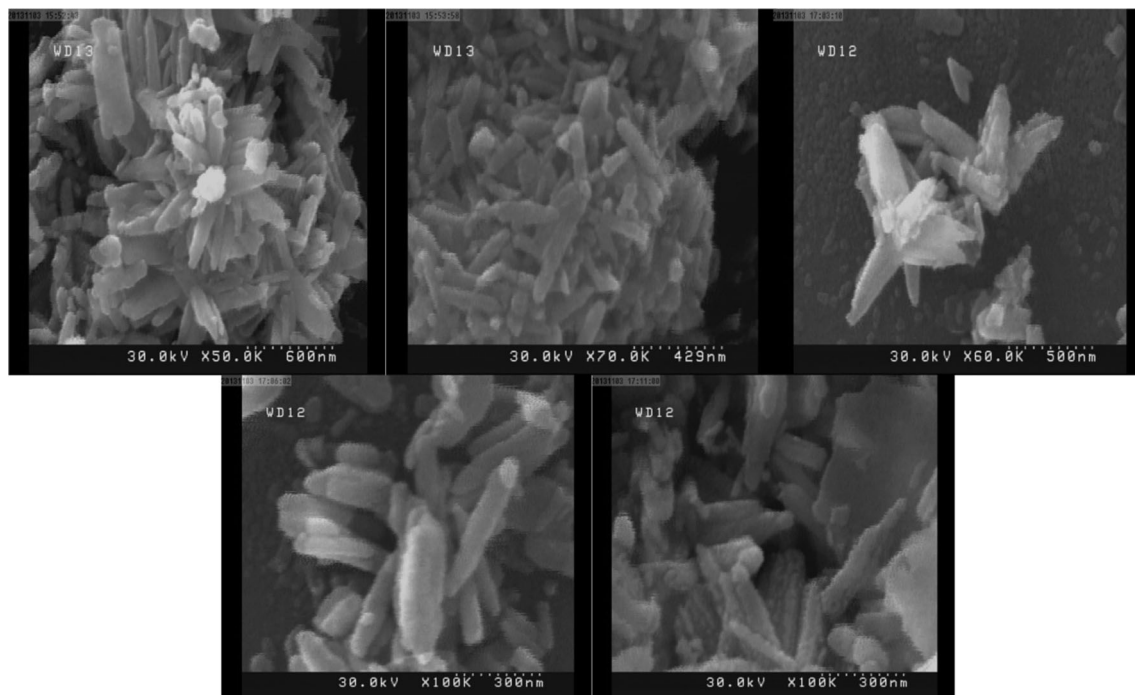


Fig. 6 FESEM of ZnO screen printed thick film prepared using hydrothermal method

optoelectronic devices; in principle, the increase in surface roughness of the films leads to a decrease in the efficiency for photovoltaic properties, therefore, it is very important

to investigate the surface morphology of the films. The AFM technique uses a laterally moving tip, while the cantilever reflects the sample's topography, or the Z

Table 1 The results from SEM measurements of ZnO film prepared at different method

Condition	Sample diameter nm	Sample length nm	Cup diameter (nm)	Thickness (μm)
<i>Sample evaporation</i>				
100 sccm	70	230	55	2
200 sccm	85	200	75	2.5
300 sccm	65	170	45	2
<i>Hydrothermal method</i>				
0.5 M	60	100	50	4

measurements. Even though the tip is very sharp, it is impossible to gather the information from the underside of specimen. The spherical particle will be viewed as a bump by the atomic force microscope. The Atomic Force microscope gives us good information about the morphology of the surface of the film. The average of grain size on the surface is found to be 100 nm and the roughness of the surface was (0.4–2.5) nm as shown in Fig. 7 (Table 2).

Study the optical properties and crystal defects of ZnO nanostructures, room temperature PL spectrum was measured and the typical spectrum is shown in Fig. 8a and b. PL is a very sensitive technique used to characterize semiconductors. During photoluminescence excitation light (in this work Xe-lamp) of energy greater than the bandgap (E_g) of the film is used to excite electrons across the band gap and into the conduction band causing an excess of electron hole pairs. These electron hole pairs (excitons) recombine within the crystal, sometimes at impurity sites as bound excitons if the semiconductor is extrinsically doped with impurities or recombine at structural defect sites or intrinsic defects and this recombination causing emission of an optically measurable photon. PL measurements have been performed in order to evaluate the optical properties of the ZnO thick films prepared by different methods and conditions. Figure 8 shows the measured PL spectra for ZnO thick films prepared by simple evaporation method with flow rates (100, 200, and 300) sccm. They consist of three peaks centered at 361, 386 and 488 nm respectively. The first peak refers to direct transition of electrons band to band, while the second band UV emission peak (386 nm) related to recombinations of free excitons, and the third is the green emission. The visible range emission of the ZnO can be attributed to radiative recombination through point defects in the ZnO lattice, such as oxygen vacancies, zinc vacancies, oxygen interstitials, and zinc interstitials. The PL intensity of all peak positions of UV emission for the ZnO 386 nm is clear and high. This suggests that the ZnO well crystalline with a wurtzite structure, while the green emission broadening refers to the defects in the film, all films green peaks have a shift towards blue shift indicating nanostructures, this agree with the XRD and SEM results. Figure 8b shows PL spectra for thick film prepared by hydrothermal method. They consist of three peaks centered at 360, 385 nm and 488 nm respectively. Corresponding to band to band, NBE, and GE respectively.

The PL intensity of peak positions of UV emission for the ZnO 385 nm is high and narrow. This indicating that the ZnO well crystalline with a wurtzite structure, while the green emission broadening refers to the defects in the film, all the films green peaks have a shift towards blue shift indicating nanostructures, this agree with the XRD and SEM results (Table 3).

3.1 Electrical measurements of constructed device

3.1.1 I-V characteristics in dark

The results of the (J-V) measurements at forward and reverse bias in dark for (n-ZnO/p-Si) devices prepared at optimum condition with different method are shown in Fig. 9. These characteristics are very important to describe the device performance and all device parameters depending on it. The (I-V) characteristics were given for two devices at optimum condition under reverse bias. It is clear that the curve contains two regions: the first is the generate where the reverse current is slightly increased with the applied voltage and this tends to generation of electron-hole pairs at low bias. In the second region, a significant increase in the reverse bias can be recognized. In this case, the current resulted from the diffusion of minority carriers through the junction. From the obtained result it is clearly that the current produce by hydrothermal method is less than that obtained from the simple evaporation method which is related to the large junction resistant which reduces the leakage current. The enhancement in the reverse current is related to enhancement in the junction structure, which results in reducing the number of defects at semiconductor-insulator-semiconductor interfaces of the two junctions. These defects results from the strain due to crystal structure, lattice parameter and probably thermal expansion mismatch. In the forward bias, the forward voltage results in reducing the height of the potential barrier, therefore, majority carriers are able to cross the potential barrier much easier than at zero bias, so that the diffusion current becomes greater than the drift current.

The results are that Fig. 9 gives the I-V characteristics behavior of the (n-ZnO/p-Si) device in the forward bias. Two regions are recognized; the first one represents recombination current, the first current established when the

Fig. 7 AFM of ZnO screen printed thick films prepared using different method
a 100 sccm simple evaporation,
b 200 sccm simple evaporation,
c 300 sccm simple evaporation and,
d hydrothermal method

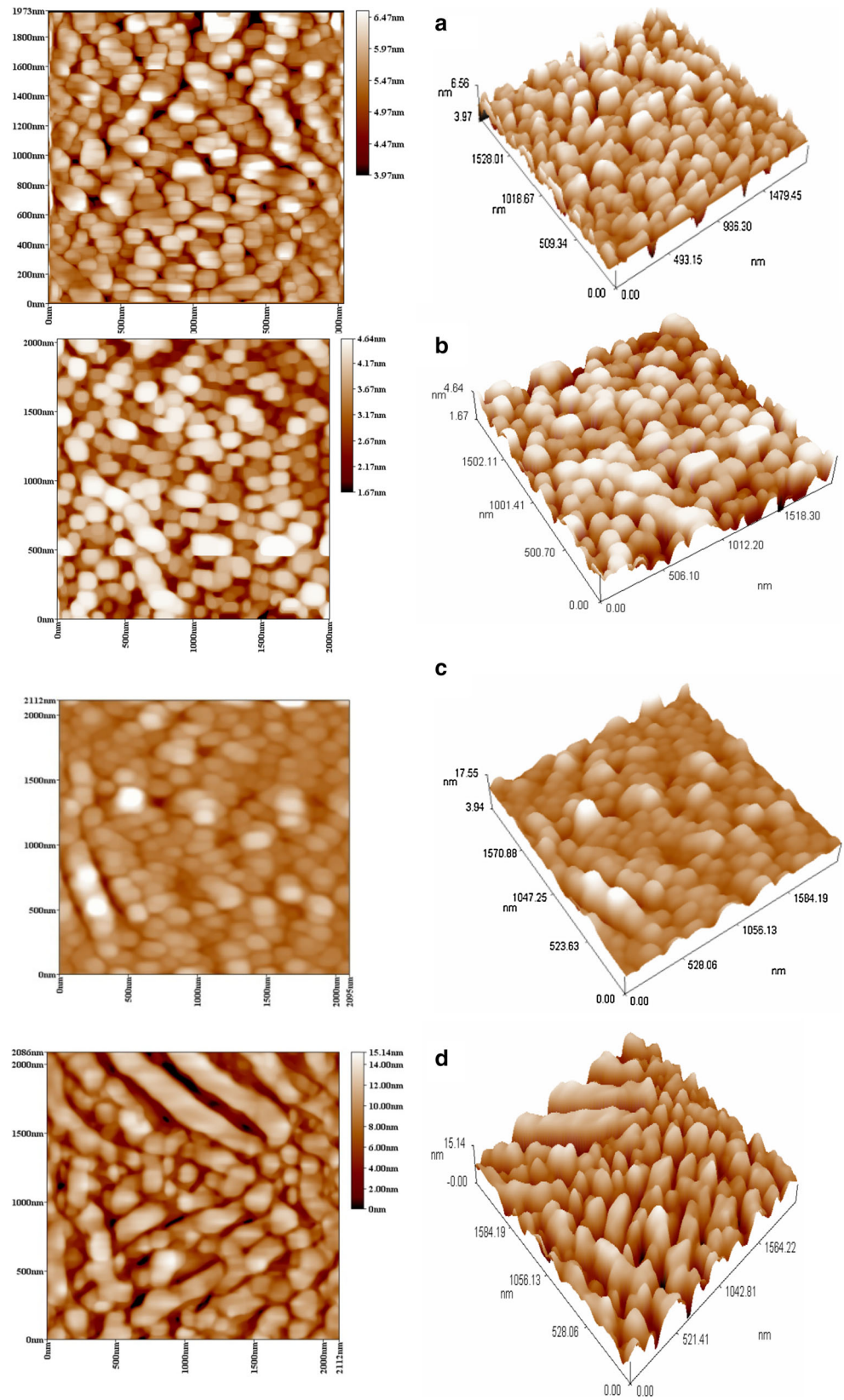


Table 2 The results from AFM measurements of ZnO screen printed films prepared at different method

Sample	Grain size (nm)	Sa (roughness average) (nm)	Sq (root mean square) (nm)	Sz (Ten point height) (nm)
<i>Simple evaporation method</i>				
100 sccm	92.23	0.416	0.531	1.62
200 sccm	84.11	0.546	0.65	1.98
300 sccm	96.76	1.02	1.38	5.25
<i>Hedrothermal method</i>				
0.5 M Zn(NO ₃) ₂ ·6H ₂ O	100.73	2.47	3	11.8

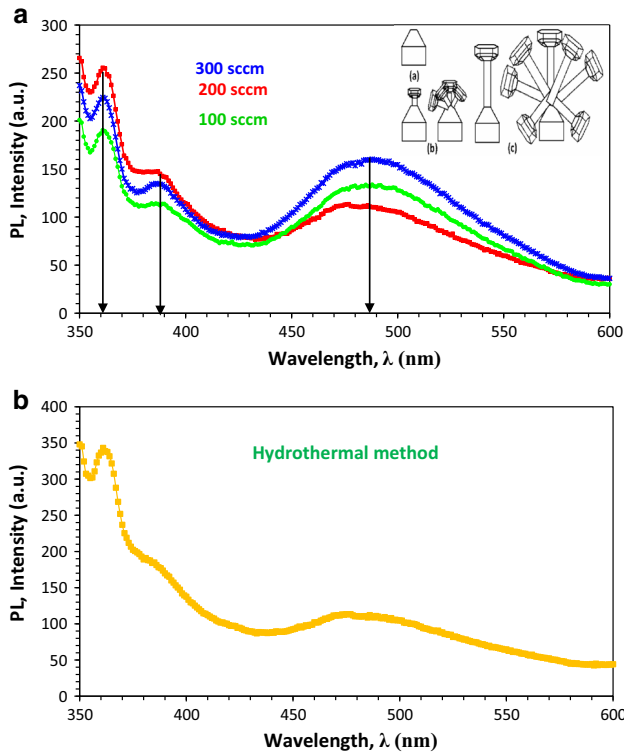


Fig. 8 PL of ZnO screen printed thick films prepared using different method **a** simple evaporation method, **b** hydro thermal method

Table 3 Values of energies estimated from PL at different wavelengths

Preparation method	E ₁ (Ev) (nm)	E ₂ (Ev) (nm)	E ₃ (Ev) (nm)
100 sccm	3.43 at 361	3.21 at 386	2.54 at 488
200 sccm	3.43 at 361	3.21 at 386	2.55 at 486
300 sccm	3.43 at 361	3.21 at 386	2.54 at 488
Hydrothermal	3.44 at 360	3.22 at 385	2.54 at 488

concentration of the generated carrier is larger than the intrinsic carrier concentration (n_i), i.e. ($n \cdot p > n_i^2$), which lead to recombination process for mass low applicable. The second region at high voltage represented the diffusion or bending region which depending on serried resistance and in (MOS) case represented the tunneling region. From the

comparison between the results obtained for both devices prepared at optimum condition, it is recognized the values of the current improved for simple evaporation method due to decrease in the resistivity for n-type ZnO film results in an increase in the electron concentration. This causes a decrease in the hole concentration and thus a reduction in I_s . The ideality factor of all devices was estimated at the optimum conditions and it has been found to be ranging around (1.97–2.76) as show in Table 4. These values refer to good rectification properties for both prepared devices. The large value of n suggests that in this voltage region, the recombination in these devices occurs primarily in the junction depletion region and at the junction interface.

Figure 9a–c exhibits the photo electric behavior of the two devices under illumination condition. It is understood that photo electric effect result from light-induced electron-hole generation at the device and particularly at the depletion region of the p-type silicon. Under external reverse bias, depletion region of the device extends and as a result, more incident photons will contribute to the electron–hole pair generation that takes place in the depletion region. The internal electric filed in the depletion region causes the electron–hole pairs to separate from each other and this bias becomes large with the applied external bias. From the following figure, we can see the increase in the photo-current with the increasing of incident light intensity, where the large intensity refers to a great number of incident photons and hence large of separated electron–hole pairs. From this result, enhancement is noticed in values of the photo current in device prepared using simple evaporation method comparing with device prepared using hydrothermal method at the same incident light intensity due to the decreased in the built-in potential, leading to a higher photo-current.

4 Conclusions

High quality of Zinc oxide nanostructures were obtained using different methods: first method (simple evaporation) at different mixture (Ar + O₂) flowing at a rate of (100, 200 and 300) (sccm) with a ratio of (10:1). And second

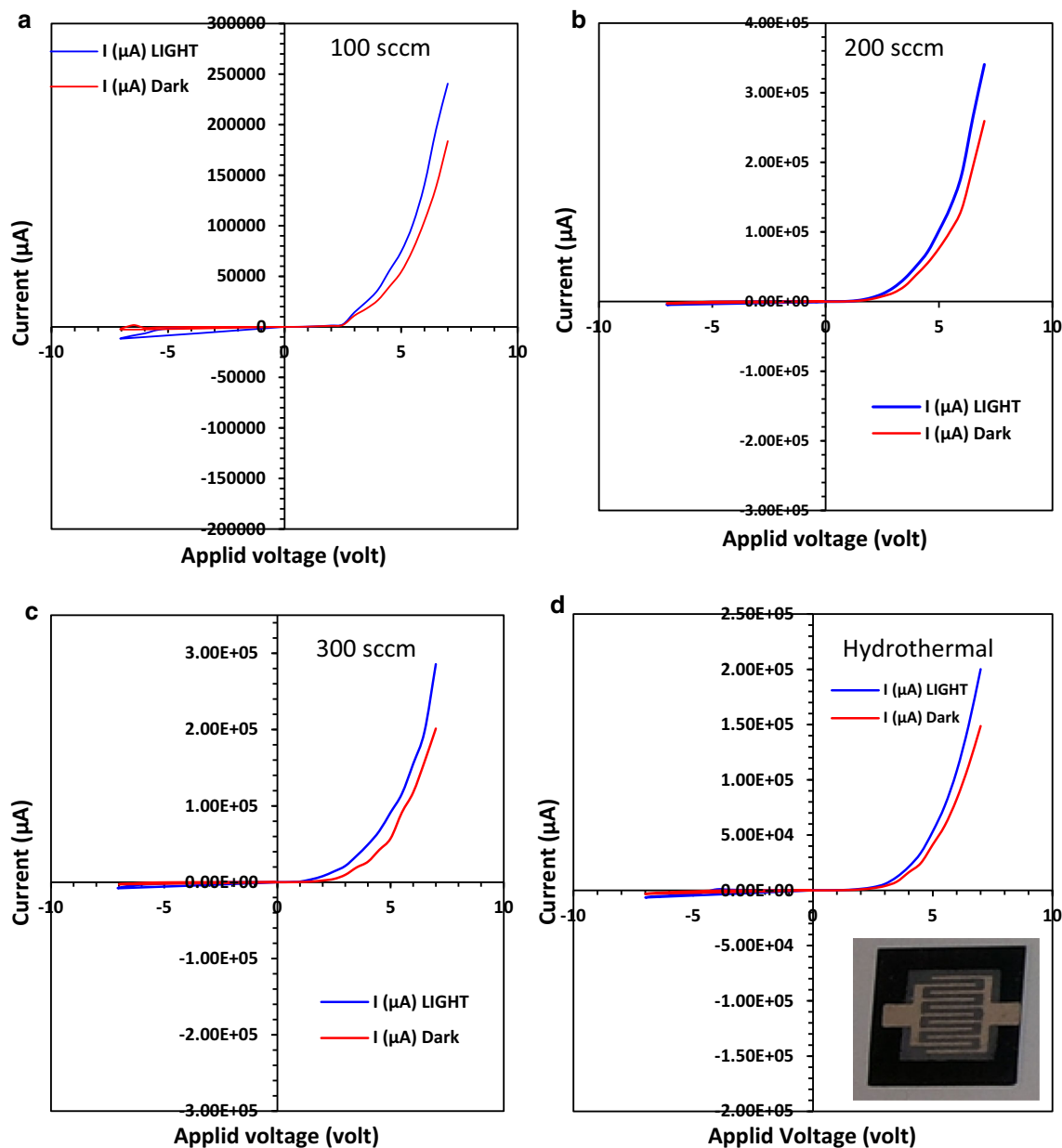


Fig. 9 I-V characteristic under forward and reverse bias of the all MOS devices **a** 100 sccm, **b** 200 sccm **c** 300 sccm, **d** hydrothermal method

Table 4 The ideality factor of all devices was estimated at the optimum conditions

Preparation method	Ideality factor
100 sccm	2.7
200 sccm	2.5
300 sccm	1.97
Hydrothermal	2.76

method (hydrothermal). X-Ray diffraction. The diffraction pattern shows strong peak at (100) and (101) plane which confirms that great amount of nanostructure has aligned on the substrate and grown with orientation along the c axis.

The average crystallite size was calculated using Scherer equation and was estimated to be about 20–30 nm. All the peaks are in good agreement with the Joint committee on powder diffraction standard (JCPDS) data belonging to hexagonal ZnO structure. It's clear that the shape and structure of the product depends strongly on the preparation conditions. The grown direction for simple evaporation method shows preferring direction while hydrothermal methods show strong growth in many directions.

Due to the high ratio of volume to surface area for nanostructures the obtained structures look very promising and effective in optoelectronic and sensing applications.

Acknowledgments The authors would like to thank Mr. Muhsin Attia, Miss. BaidaMuhsen, Mr. AsaadMjbland Mr. Ali Jasim for their assistance and supporting.

Open Access This article is distributed under the terms of the Creative Commons Attribution License which permits any use, distribution, and reproduction in any medium, provided the original author(s) and the source are credited.

References

1. X.Y. Kong, Z.L. Wang, Spontaneous polarization-induced nanohelices, nanosprings, and nanorings of piezoelectric nanobelts. *Nano Lett.* **3**, 1625 (2003)
2. Y.H. Leung, A.B. Djurii, J. Gao, M.H. Xie, Z.F. Wei, S.J. Xu, W.K. Chan, Zinc oxide ribbon and comb structures: synthesis and optical properties. *Chem. Phys. Lett.* **394**, 452 (2004)
3. F. Liu, P.J. Cao, H.R. Zhang, J.Q. Li, H.J. Gao, Controlled self-assembled nanoaeroplanes, nanocombs, and tetrapod-like networks of zinc oxide. *Nanotechnology* **15**, 949 (2004)
4. P.-A. Hu, Y.-Q. Liu, L. Fu, X.-B. Wang, D.-B. Zhu, Creation of novel ZnO nanostructures: self-assembled nanoribbon/nanoneedle junction networks and faceted nanoneedles on hexagonal microcrystals. *Appl. Phys. A* **78**, 15 (2004)
5. H. Zhang, D. Yang, S. Li, X. Ma, Y. Ji, J. Xu, D. Que, Controllable growth of ZnO nanostructures by citric acid assisted hydrothermal process. *Mater* **1**
6. M.H. Huang, S. Mao, H. Feick, H. Yan, H. Kind, E. Weber, R. Russo, P. Yang, *Science* **292**, 1897 (2001)
7. H.D. Li, S.F. Yu, S.P. Lau, E.S.P. Leong, H.Y. Yang, T.P. Chen, A. Abiyasa, C.Y. Ng, *Adv. Mater.* **18**, 771 (2006)
8. S.K. Marathe, P.M. Koinkar, S.S. Ashtaputre, M.A. More, S.W. Gosavi, D.S. Joag, S.K. Kulkarni, *Nanotechnology* **17**, 1932 (2006)
9. W.W. Wang, G.M. Zhang, L.G. Yu, X. Bai, Z.X. Zhang, X.Y. Zhao, *Physica E* **36**, 86 (2007)
10. M.H. Zhao, Z.L. Wang, C.X. Mao, *Nano Lett.* **4**, 587 (2004)
11. M. Senthil Kumar, D. Chhikara, K.M.K. Srivatsa, Structure-controlled growth of ZnO nanonails by thermal evaporation technique. *Cryst. Res. Technol.* **46**(9), 991–996 (2011). doi:[10.1002/crat.201100141](https://doi.org/10.1002/crat.201100141)
12. G. Shen, Y. Bando, C.-J. Lee, Synthesis and evolution of novel hollow ZnO Urchins by a simple thermal evaporation process. *J. Phys. Chem. B* **109**, 10578–10583 (2005)